



Enhancing sustainability in Inconel 718 machining: temperature control with internally cooled tools

Gustavo Henrique Nazareno Fernandes^{1,2} · Lucas Melo Queiroz Barbosa¹ · Pedro Henrique Pires França¹ · Eduardo Ramos Ferreira¹ · Paulo Sérgio Martins³ · Álisson Rocha Machado^{1,4}

Received: 22 July 2023 / Accepted: 8 September 2023 / Published online: 25 September 2023
© The Author(s), under exclusive licence to Springer-Verlag London Ltd., part of Springer Nature 2023

Abstract

Out of all the mechanical energy generated during material cutting, the majority is converted into heat, raising the temperature at the chip-tool interface, particularly in difficult-to-machine materials like Inconel 718, thereby diminishing tool lifespan. Consequently, various lubri-cooling methods mitigate issues related to high temperatures, such as reduced tool life and geometric distortions. The most employed method is cutting fluids application (CFA), but this approach poses several problems, including high cost and environmental and operator hazards. As a result, several techniques have been developed to lower machining temperatures, such as minimum quantity lubrication (MQL), cryogenics, and indirect tool cooling. In this study, an innovative method of tool cooling via internally cooled tool (ICT) was devised and tested. In this approach, the cooling fluid circulates in a closed loop without direct contact with the workpiece or even any fluid dispersion to the atmosphere, increasing environmental appeal and reducing manufacturing coasts. The developed method was compared with temperature measurements taken through thermography and a tool-workpiece thermocouple during the turning of Inconel 718. Two factorial designs studied temperature in Inconel 718 turning via thermocamera and tool-workpiece thermocouple. Additionally, the tool coating (TiNAl or AlCrN + TiNAl), cutting speed, feed, and depth of cut were varied. Using the tool-workpiece thermocouple method, ICT and CFA did not observe any statistically significant temperature difference. However, between ICT and DM, ICT exhibited a lower temperature at the tool-workpiece interface. With thermal imaging, ICT displayed a lower chip temperature than DM. In sum, internally cooled tools emerge as an innovative and environmentally sustainable solution for machining Inconel 718. They offer outstanding heat removal capabilities and substantial advantages over cutting fluids while significantly surpassing the performance of dry machining, thereby addressing crucial concerns in sustainable machining practices.

Keywords Inconel 718 · Nickel-based superalloy · Internally cooled tools · Tool-workpiece thermocouple system · Thermocamera · Tool coating · Eco-friendly machining

✉ Gustavo Henrique Nazareno Fernandes
ghnfernandes@gmail.com

¹ Faculty of Mechanical Engineering, Federal University of Uberlândia - UFU, 2121, João Naves de Ávila avenue, Campus Santa Mônica, Uberlândia, MG 38408-100, Brazil

² University of South Australia – UniSA, Mawson Lakes, SA 5095, Australia

³ Fiat Chrysler Automobiles - FCA, Manufacturing Engineering, Betim, MG 32.669-900, Brazil

⁴ Mechanical Engineering Graduate Program, Pontifícia Universidade Católica do Paraná–PUCPR, Rua Imaculada Conceição, 1155, Prado Velho, Curitiba, PR 80.215-901, Brazil

1 Introduction

Machining is a complex manufacturing process in which a significant amount of heat flows into the tool, thereby increasing the temperature at the chip-tool interface. For instance, Inconel 718 machining can reach over 1000 °C [1]. The foundational understanding of heat distribution within the cutting system traces its origins to the pioneering work of Schmidt and Roubik [2], who conducted an insightful calorimetric investigation into the machining process. The authors provided a representative illustration of the characteristic heat distribution across critical elements, including the workpiece, the cutting tool, and the resulting chips, concerning variations in cutting speed.

Remarkably, this fundamental insight has withstood the test of time and remains a bedrock principle in metal cutting. A broad spectrum of contemporary references spanning several authoritative texts, including those authored by Shaw [3], Kronenberg [4], Klocke [5], and Grzesik [6], resoundingly reaffirm and extend the validity of these findings. This consensus underscores the significance of Schmidt and Roubik's pioneering work in shaping the understanding of heat distribution in machining processes and its continued relevance in modern metal-cutting practices.

Several studies have highlighted the adversities of high temperatures in the machining process. These include (i) reduction in tool life; (ii) unwanted deformations; (iii) loss of dimensional accuracy; (iv) impaired surface integrity, such as increased roughness, excessive hardening, thermal cracks, and poor visual effects; and (v) productivity limitations and increased costs. Various research studies have documented these adverse effects [1, 7].

Inconel 718, a widely used superalloy, presents specific challenges related to high-temperature machining. This nickel–chromium–iron alloy contains significant amounts of niobium, molybdenum, titanium, and tantalum, making it a popular choice in the industry [8, 9]. However, machining this material poses difficulties due to its low thermal conductivity, high mechanical resistance at elevated temperatures, and chip formation that concentrates heat at the tool tip. These factors collectively contribute to rising temperatures exceeding 1000 °C [10, 11]. As a result, addressing the issues associated with high temperatures becomes even more crucial when working with Inconel 718. Due to the aforementioned factors, Inconel 718 machining occurs at lower cutting speeds than other metals, with values up to 100 m/min in most cases and, in specific cases, up to 150 m/min with carbide tools. In the case of ceramic tools, references can be found for turning processes with speeds of up to 300 m/min. Additionally, the feed and depth of cut are relatively low, with studied values of up to 0.25 mm/rev and 1.5 mm, respectively. Due to the requirement for cooling, wet machining or MQL is commonly employed in turning. However, other methods, such as cryogenic machining, are also being investigated [12, 13]. With ceramic tools, the standard practice is cutting dry [2, 11].

Coolant flood application decreases the temperature and lubricates the chip-tool interface. They prevent overheating, lubricating, avoiding corrosion, and flushing away chips—making them crucial for machining operations [14–16]. Iturbe et al. [17] compared two lubri-cooling techniques, minimum quantity lubrication with cryogenics and CFA, during the machining of Inconel 718. Cutting fluids improved tool life compared to MQL with cryogenics.

Cutting fluids should be disposed of properly to prevent harmful environmental effects [18] and human health [19–21]. They can contaminate soil and waterways and

endanger animal life [22, 23]. Cutting fluids also contribute to manufacturing costs, making eco-friendly alternatives necessary [16, 24]. There are several approaches to mitigate the environmental impacts arising from cutting fluid [25]. Some studies aim to modify its origin using plant-based cutting fluids [26], potentially reducing the fluid volume used through techniques such as MQL, where the fluid is sprayed by compressed air [27, 28]. This method can be enhanced by incorporating nano lubricants [25, 29, 30]. Other potential methods involve the elimination of cutting fluids, such as the application of cryogenic techniques [31], compressed air [32], or heat pipes [33, 34].

At least since 1964, when Meyers [35] patented a thermoelectric system specifically designed for the cutting tool, alternative cooling methods have been developed to reduce or eliminate the need for cutting fluids. Later, in 1970, Jeffries and Zerkle [36] expanded on this concept by presenting a mathematical thermal analysis of an indirectly cooled tool in orthogonal cutting and received a patent for this device in 1971 [37].

Since then, many efforts to reduce cutting fluid usage have led to innovative cooling techniques focusing on the tool [16]. Studies, such as those by Barbosa [38], Fernandes et al. [39], and Wei [40], have explored effective tool cooling methods. Rozzi et al. [41] also successfully used liquid nitrogen to enhance tool life while turning AISI 416 stainless steel with their tool-coupled heat exchangers.

In the same line, França [42] found that during gray cast iron turning, indirectly cooled turning (ICT) reduced temperatures by up to 21.52% compared to dry machining (DM). This was achieved by injecting cold water without direct contact with the workpiece. Peixoto's study [43] found that using a particular cooling design resulted in a 21% decrease in cutting force and a 15% improvement in surface roughness (R_a) compared to dry machining, providing valuable insights for machining purposes.

Barbosa [38] conducted a study on turning AISI D6 steel and found that indirectly cooled turning (ICT) reduced tool temperature, resulting in a 35% increase in tool life. Although cutting force increased during ICT, reduced thermal softening improved tool performance. Dry machining with limited cooling leads to higher temperatures and increased wear.

Despite conducting an extensive search in renowned journal databases such as Web of Science, Clarivate, Scopus, and Science Direct, no prior studies were discovered that have investigated the application of an internally cooled system (ICT) in the machining of Inconel 718. This notable absence indicates a significant research gap in this area.

This project is undertaken with the overarching aim of developing and rigorously assessing a novel eco-friendly machining cooling method. The primary objective is to systematically evaluate the performance of this innovative technique, referred to as Internal Channel Cooling (ICT), with a specific focus on temperature dynamics, given its

pivotal role and potential impact on the overall manufacturing process. The study addresses a critical gap in the existing literature by introducing an inventive cooling approach applied to the machining of Inconel 718.

In this approach, cemented carbide cutting tools were internally cooled via precisely crafted channels created through wire electrical discharge machining (WEDM). A mixture of water and monoethylene glycol within these channels circulates at sub-zero temperatures. The study rigorously tests the ICT system in the turning process of Inconel 718 to advance sustainable machining practices. The comparative analysis involves benchmarking ICT against traditional coolant flood application and DM methods.

The primary focus centers on the cutting temperature, a pivotal output variable. Two distinct measuring techniques are employed: a thermal imaging camera captures real-time temperature data of the moving chip across the tool's rake face, and a tool-workpiece thermocouple precisely gauges the temperature at the chip-tool interface. The findings from the internally cooled tools are comprehensively compared against those from dry machining and coolant flood application.

This research endeavors to provide valuable insights into the efficacy of ICT as a sustainable machining solution, offering a viable alternative to traditional methods in terms of both performance and environmental impact.

2 Methodology

In this section, all procedures and materials employed will be elucidated. Firstly, the machined material, Inconel® 718, and its chemical and mechanical properties will be introduced. Subsequently, the entire system of internally cooled tools (ICT) developed for this study will be comprehensively expounded upon, including the employed tools. Furthermore, the statistical planning and methodology employed in the analyses and the utilized equipment will be meticulously delineated.

2.1 Materials and tools

A Villares Metals SA bar labeled VAT718 A, made of Inconel 718®, was used in the study. The alloy underwent thermal treatment before machining. Table 1 has more information on the material. Figure 1 shows niobium and titanium carbides as white points and minimal delta phase as dark points in the microstructure of Inconel 718. This material was selected due to its low machinability, as it experiences high temperatures at the interface, low thermal conductivity, and maintains strength at elevated temperatures.

A conventional refrigerator was modified to cool the tools internally using a mixture of water and mono-ethylene

glycol. The temperature was maintained at approximately -5°C . Channels were created within the tools using an electric discharge machine (EDM) to circulate the coolant. The carbide inserts (SNMG 120408EN-M34 CTPX710) and tool holder (DSSNR2525X12-P) were adapted to allow internal fluid circulation. Figure 2 visually depicts the tool holder/insert set with cooling channels, while Table 2 provides detailed specifications of the cooling systems.

The internally cooled tool (ICT) system includes a cutting tool with internal cooling channels, a tool holder, a coolant pump, a reservoir, and a cooling system to control the temperature. Water was used as the coolant, maintained at -5°C . Figure 2 illustrates the coolant flow from the reservoir through the tool holder, reaching the top of the tool. The coolant removes heat from the cutting process and returns to the reservoir.

Ceratizit's ISO SNMG 120408EN-M34 CTPX710 carbide inserts were used in the machining experiments. Two variations were tested: one with a TiAlN coating and another with a AlCrN over TiAlN double coating. Inserts with and without internal channels were also examined, resulting in four different configurations. Table 3 provides detailed information on these configurations and their characteristics, offering an overview of the insert tips used in the experiments.

The ISO SNMG 120408EN-M34 CTPX710 tools are typically coated with TiAlN. However, to machine Inconel 718, Oerlikon Balzers® recommended Balinit® AlCrN as the most suitable coating. Therefore, in this study, the tools were tested with both the single layer TiAlN and the AlCrN over TiAlN double layer coating. The combination of AlCrN over TiAlN is called AlCrN+ to simplify the terminology.

For the coolant flood application, a water emulsion named ECO COOL P 1977 BF, manufactured by *Fuchs Lubricants do Brasil Ltda*, was used. This emulsion is mineral oil and boron-free. The emulsion was prepared by mixing 25% of the fluid with 75% conventional water (tap water). The concentration of the emulsion was measured using a bench refractometer (Atago, model Pocket PAL-1).

The internally cooled system utilized a coolant fluid composed of a homogeneous mixture of water and monoethylene glycol. The use of mono-ethylene glycol served two primary purposes. Firstly, it acted as an anticorrosive agent, preventing corrosion issues within the cooling system. Secondly, it provided anti-freezing capabilities, allowing the mixture to function below 0°C . The coolant mixture consisted of 90% water and 10% mono-ethylene glycol, ensuring efficient cooling from the internal system to the cutting tool.

2.2 Machining and design of experiment

Initially, the experimental plan aimed to analyze temperature using a thermocamera and a tool-workpiece thermocouple

Table 1 Composition, mechanical, and physical–chemical properties of Inconel 718 [9, 44]

Composition	Ni	Cr	Fe	Nb	Mo	Ti	Al	C	Co
Inconel 718 (aged/precipitated)	52.90	18.48	18.88	5.11	2.94	0.98	0.54	0.032	0.04
Mechanical properties									
Alloy	Ultimate tensile strength (MPa)	Yielding limit (0.2%) (MPa)	deformation in 50 mm (%)	Modulus of elasticity (GPa)	Hardness (HRC)				
Inconel 718 (aged/Precipitated)	1240	1036	12	211	40				
Physico-chemical properties									
Density (g/cm^3)	Melting point range ($^{\circ}C$)	Specific heat ($J/kg.K$)	Avera. thermal expansion coefficient ($\mu m/m.K$)	Thermal conductivity ($W/m.K$)	Electrical resistivity ($\eta\Omega m$)	Curie temperature ($^{\circ}C$)			
Inconel 718 (aged/precipitated)	8.19	1260~1336	435	13.0	11.4	1250	-112		

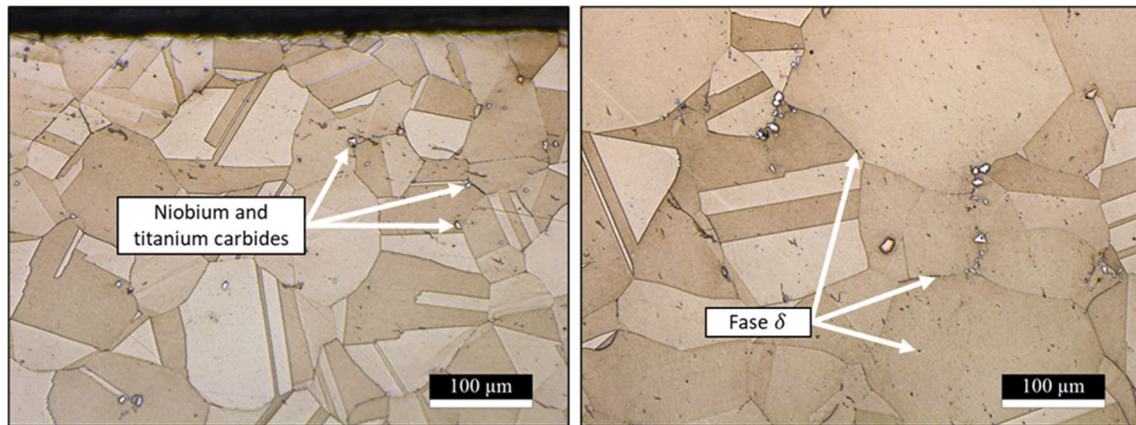


Fig. 1 Microstructure of Inconel 718.® VAT718 A produced by Villares Metals SA. Periphery zone (left) and center (right)

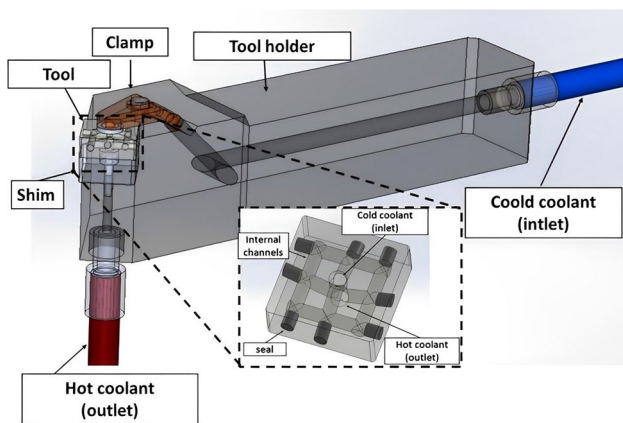


Fig. 2 Tool holder set, and cemented carbide insert made by (EDM)

Table 2 Specifications of the refrigeration system [39]

Commercial freezer (make/model)	Prosdocimo/04180CBC201
Cooling capacity [W]	146
The coolant of the chiller	R 134
The coolant of the tool	Water (90%) Mono ethylene glycol (10%)
Minimum temperature [°C]	−5
Reservoir capacity [l]	60
Flow [l/min]	1.02
Coolant pressure [KPa]	700

system simultaneously. The first Design of Experiments (DoE) utilized a $2^{(5-1)}$ fractionated factorial design. Table 4 lists the variables with two levels (− and +). The input variables, included cutting speed (v_c) at 47 and 94 m/min, feed (f) at 0.1 and 0.2 mm/rev, depth of cut (doc) at 0.25 and 0.5 mm, atmosphere (ICT, DM, and CFA), and coating (TiAlN and AlCrN+).

Higher machining parameter values were deliberately selected to stress the modified inserts with internal channels and evaluate their durability. Despite the manufacturer’s 40 m/min cutting speed for Inconel 718, a 94 m/min value was used to significantly increase the temperature and thoroughly analyze the ICT behavior.

A second fractionated DoE was conducted using a $2^{(5-1)}$ design, varying only the cutting atmosphere between ICT and CFA. Thermal camera tests were performed for DM and ICT conditions, as the method is unsuitable for CFA. Forty-eight experiments were conducted for temperature analysis, including initial tests (T1) and one replicate (T2). For more information about each test, refer to Table 5.

2.3 Temperature measurements

Two ways to measure the temperature during the machining process are via a thermocamera, which uses infrared sensors, and the tool-workpiece thermocouple system. The infrared radiation measuring technique assumes that any object surface with a temperature above absolute zero (-273°C) emits electromagnetic radiation in the infrared (IR) spectrum with a wavelength varying between $1\text{ to }100\mu\text{m}$. This effect was initially observed by the English physicist William Herschel in 1800 when measuring the temperature of a crystal’s light spectrum using a mercury thermometer. The scientist noticed that the heat was more intense near the red-light spectrum, but there was no visible light [46].

Based on these principles and intense technological development, it is currently possible to use high-precision capture infrared cameras. This method is widely used in machining and has several advantages: (i) it is non-intrusive; (ii) modern devices have high data acquisition rates; (iii) it has high measurement accuracy; (iv) it allows measurements in hard-to-reach locations; (v) relatively easy to apply

Table 3 Cemented carbide tools specifications [45]

Tool				
Standard ISO Code	SNMG 120408EN-M34 CTPX710			
Internally Cooled Tool	No	Yes	No	Yes
Coating	TiNAl	TiNAl	Balinit® ALCRN +	Balinit® ALCRN +
Available cutting edge	8			
Insert angle	90 °			
Inscribed circle diameter	12.7 m			
Cutting edge length	12.9 m			
Fixing hole diameter	5.76 m			
Insert width	4.76m			
Tip radius (r_ϵ)	0.8 mm			
Feed (f)	0.1 – 0.35 $\frac{mm}{rev}$			
Depth of cut (doc)	0.1 – 3.5 mm			
Cutting speed (v_c)	40 $\frac{m}{min}$			
Chip breaker	M34			

Table 4 Temperature experimental planning with five variables

Factors	Variables	Levels		Atmosphere y_5
		(-)	(+)	
Cutting speed (v_c) [m/min]	y_1	45	90	ICT, DM, or CFA
Feed (f) [mm/volt]	y_2	0.103	0.297	
Coating	y_3	ALCrN +	TiNAl	
Depth of cut (a_p) [mm]	y_4	0.25	0.50	

compared to other methods; (vi) measuring temperature along the surface, i.e., it is not just at a point.

This method identifies the maximum temperature within the infrared camera frame, specifically on the upper chip surface, as determined through thermocamera analysis [47]. It is important to emphasize that the maximum temperature recorded by the thermocamera primarily reflects temperatures on the chip's upper free surface. This temperature reading may not precisely correspond to the maximum cutting temperature occurring at the tool-chip interface, which is subject to variations in chip thickness due to different cutting feeds and changes in chip-free surface configurations with varying cutting speeds. While the infrared camera method provides

valuable temperature data, its limitations should be considered when interpreting the results, especially concerning variations in feed and cutting speeds.

The infrared thermocamera limitations encompass (i) challenges in accurately determining surface emissivity values; (ii) the possibility of camera obstruction due to chip accumulation or interference from cutting fluids; (iii) the critical necessity for precise camera positioning; (iv) the ability to record temperatures solely on external surfaces; and (v) its intrinsic limitation in directly quantifying the cutting temperature at the tool-chip interface. Instead, an infrared camera predominantly captures temperatures at the chip's free surface [48–50].

Table 5 Fractionated factorial experiment design (2^{5-1})

Test	Atmosphere	Coating	Depth of cut [mm]	Feed [mm/rev]	Cutting speed [m/min]
1	DM	TINAL	0.25	0.103	47
2	ICT	TINAL	0.25	0.103	94
3	ICT	TINAL	0.50	0.103	47
4	DM	TINAL	0.50	0.103	94
5	ICT	TINAL	0.25	0.297	47
6	DM	TINAL	0.25	0.297	94
7	DM	TINAL	0.50	0.297	47
8	ICT	TINAL	0.50	0.297	94
9	ICT	ALCRN+	0.25	0.103	47
10	DM	ALCRN+	0.25	0.103	94
11	DM	ALCRN+	0.50	0.103	47
12	ICT	ALCRN+	0.50	0.103	94
13	DM	ALCRN+	0.25	0.297	47
14	ICT	ALCRN+	0.25	0.297	94
15	ICT	ALCRN+	0.50	0.297	47
16	DM	ALCRN+	0.50	0.297	94
17	CFA	TINAL	0.25	0.103	47
18	CFA	TINAL	0.50	0.103	94
19	CFA	TINAL	0.25	0.297	94
20	CFA	TINAL	0.50	0.297	47
21	CFA	ALCRN+	0.25	0.103	94
22	CFA	ALCRN+	0.50	0.103	47
23	CFA	ALCRN+	0.25	0.297	47
24	CFA	ALCRN+	0.50	0.297	94

Meola and Carlomagno [46] feature the calibration function of a camera term, Eq. 1:

$$E = \epsilon \frac{A}{(e^{B/T} - C)} \tag{1}$$

where:

- ϵ = emissivity coefficient of a surface;
- T = is the temperature of the object through calibration constants A, B, C.

Since Planck’s law gives the radiation intensity of a black body as a function of temperature (T) and wavelength (λ), Eq. 2 [51]:

$$E(\lambda, T) = \frac{C_1}{\lambda^5 (e^{(C_2/\lambda T)} - 1)} \tag{2}$$

where:

- λ = wavelength in m;
- T = the temperature of the object in K;
- C_1 and C_2 = First and second constant radiation,
- $C_1 = 1.191044 \times 10^{-16} \text{Wm}^2$ and $C_2 = 0.014388 \text{ m.K.}$

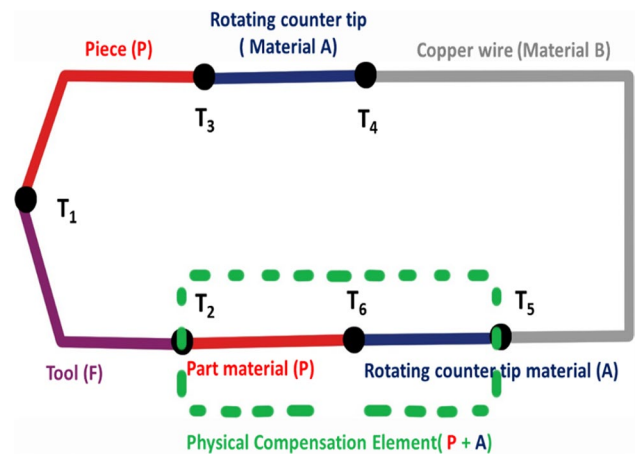


Fig. 3 Schematic representation of the tool-workpiece thermocouple system with a physical compensation element [39]

However, a real body emissivity constitutes only a fraction of an ideal black body emissivity, considering an equal temperature and wavelengths. Thus, Eq. 3 [46]:

$$\epsilon_\lambda = \frac{E_\lambda}{E_{(\lambda, T)}} \tag{3}$$

where;

- L_λ = intensity of reading a real body;
- $L_{(\lambda, T)}$ = radiation intensity of an ideal black body.

Following Seebeck’s law, the tool-workpiece thermocouple bench is formed by a thermoelectric system that involves a chain of elements and several junctions besides the one developed by the tool insert and the workpiece. According to Kaminise et al. [52], adding a physical compensation to minimize the effect of the electromotive forces (e.fs) caused by cold joints is possible. The various cold joints (T2 to T6) generate a voltage by adding a component formed by two materials in the circuit that compose the standard measurement system. The physical compensation element comprises the counter tip material A and workpiece material P, as shown in Fig. 3. It also allows calibration on the test bench, which is carried out externally in most cases and may not represent the system more realistically adequately.

Analyzing the standard circuit with the addition of the physical compensation element, Eq. 4 is obtained:

$$\Delta E = E_{FP} \cdot T_1 + E_{PA} \cdot T_3 + E_{AB} \cdot T_4 - E_{AB} \cdot T_5 - E_{PA} \cdot T_6 - E_{FP} \cdot T_2 \tag{4}$$

When considering that the cold joints distant from the cutting zone do not present temperature variations throughout the tests, the temperature relations will be $T_3 = T_4 = T_5 = T_6$, Eqs. 4, 5 and 6:

$$E_{PA} \cdot T_3 = E_{PA} \cdot T_6 \text{ and } E_{AB} \cdot T_4 = E_{AB} \cdot T_5 \quad (5)$$

Thereby,

$$\Delta E = E_{FP} \cdot T_1 - E_{FP} \cdot T_2 = K(T_1 - T_2) \quad (6)$$

Finally, isolating T_1 , the final Eq. 7 will be given by:

$$T_1 = T_2 + \frac{\Delta E}{K} \quad (7)$$

Note that, by Eq. 7, it is possible to obtain the cutting temperatures by the voltage ΔE measured by a voltmeter, where T_1 is the average temperature obtained at the chip-tool interface, T_2 is the joint temperature formed by the contact of the element compensation in the tool, and K is the Seebeck constant obtained in the system calibration [52]. The temperatures obtained in T_2 can vary throughout the cutting process [53]. Therefore, it is necessary to measure T_2 during the calibration and execution of the tests and, hence, during the development of the final curve.

The tool-workpiece thermocouple system offers several advantages: (i) it provides real-time temperature data during machining, allowing for a dynamic understanding of temperature fluctuations; (ii) it offers localized temperature measurement at the tool-chip interface, which is crucial for gaining insights into specific heat generation zones and optimizing machining processes; (iii) it is relatively cost-effective when compared to advanced temperature measurement techniques, making it accessible for a wide range of machining operations; (iv) it boasts a simple setup, requiring minimal specialized equipment or expertise, which enhances its usability [42, 52].

However, there are certain drawbacks associated, such as (i) one significant limitation is its restricted spatial resolution, as it may not capture temperature variations across the entire cutting region, potentially leading to inaccuracies in temperature assessment; (ii) determining the exact temperature, if maximum or average, can also be challenging, and there is no consensus in the literature [54]; (iii) calibration of the system can be difficult and not precisely reflect the real machining conditions; and (iv) the system is subject to eddy currents that can affect measurement accuracy.

For temperature measurements, a thermocamera FLIR Tools® model A325 was used, with a resolution of 320×240 pixels and a temperature range of 300 to 1200 °C (± 2 °C accuracy). The acquisition rate was 30 frames per second, and the emissivity value for nickel alloy was $\epsilon = 0.35$. A single fractionated factorial design $2^{5(5-1)}$ was employed for the thermal camera analysis, with 32 runs, including replicas. The measurements were performed on new tools with maximum flank wear kept below 0.1 mm ($V_{Bmax} < 0.1$ mm). The thermal camera was positioned to focus on the upper chip surface, measuring 45 s per frame. The average maximum

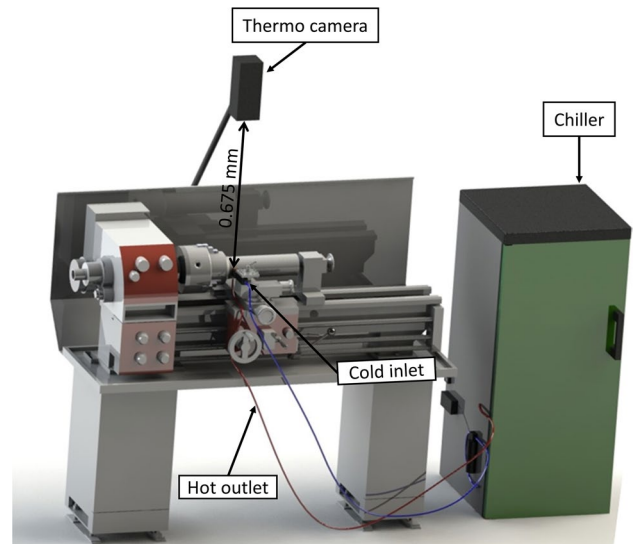


Fig. 4 Temperature experiment setup with a thermal camera and tool-workpiece thermocouple system

temperature per frame was calculated using FLIR ThermoCAM researcher professional 2.10 software, with a focal distance of 0.675 m, as shown in Fig. 4.

Temperature measurements were conducted using the thermocamera and the tool-workpiece thermocouple method. The tool-workpiece thermocouple system was tested for all three conditions (ICT, DM, and CFA) on an IMOR MAX II universal lathe. Each machining test lasted approximately 45 s to reach a steady-state temperature.

Data signals generated during machining were captured using an Agilent® 34901A data acquisition board with high resolution (1 μ V) and low measurement uncertainty (0.3 °C). Sampling was done at a frequency of 2 Hz for accurate measurements. The thermoelectric circuit of the tool-work thermocouple was connected to the modified rotation counter tip and the compensation element through copper wires.

Figure 5 depicts the experimental setup for temperature measurements using both methods, with electrical isolation of the bar and tool holder to prevent signal loss due to electrical interference.

An internally modified live center was utilized in the lathe's tailstock to facilitate the transfer of electrical signals from the rotating workpiece. Within this live center, a Teflon® capsule was incorporated, which contains liquid mercury. The liquid mercury is in contact with the rotating conical point inside the live center, ensuring the continuity of the electrical signal during the tests. Electrical isolation is maintained between the live center's fixed cone and the tailstock's mandril to prevent interference.

The rotating conical point, composed of SAE 1050 steel, captures the electrical signal from the rotating workpiece and transfers it to the liquid mercury. The liquid mercury, in turn,

Fig. 5 Experimental assembly diagram for temperature measurement

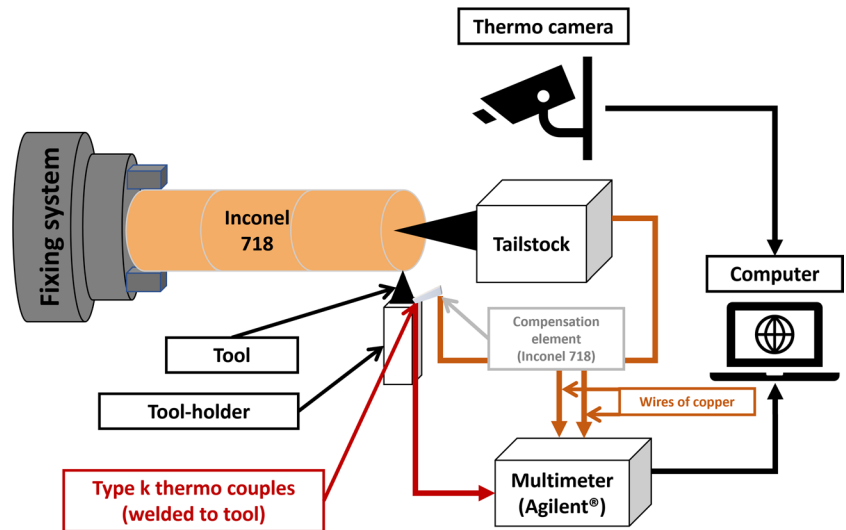
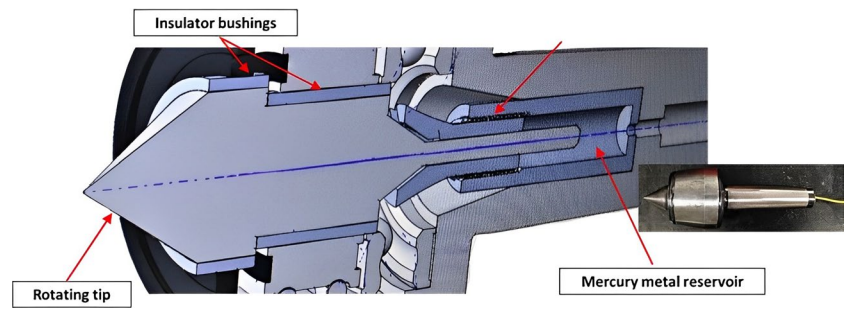


Fig. 6 Modified mandril of the tailstock for capturing the signal of a rotating part used [42]



transmits the electrical signal to an embedded copper wire, thereby completing the circuit for the measurement system. For reference, Fig. 6 illustrates a similarly modified tailstock an example.

The calibration of the tool-workpiece thermocouple followed a methodology similar to that used by other researchers [55, 56]. A thermocouple was constructed using a piece of Inconel 718 ribbon chip and a cemented carbide insert. Copper wires were soldered to the ends of the thermocouple. Additionally, a K-type thermocouple (nickel–chromium/nickel–alumel) with a temperature measuring range of -200 to 1260 °C was positioned very close to the tip of the chip-tool thermocouple.

To calibrate the thermocouples, they were placed in an electric induction oven of the Mufra type with a power output of 7500 W. The oven was heated, and the temperatures of the thermocouples were monitored. This calibration method offers the advantage of achieving an excellent correlation between temperature and electromotive forces (e.fs.). It considers the secondary junctions present in the tool-workpiece thermocouple system. Figure 7 provides a schematic representation of the experimental setup used for the calibration process.

The calibration involved fixing the Inconel 718 chip and cemented carbide bar to form the reference joint. A type K thermocouple was inserted adjacent to this joint to measure calibration temperatures. The electrical signals generated by the chip-tool thermocouple were collected and correlated with the temperatures measured by the K-type thermocouple. The entire system was electrically closed and insulated for accurate calibration. Calibration curves were generated based on these measurements. Although different equipment was used for calibration, the principles of Seebeck's law were followed, ensuring an accurate representation of temperatures during machining.

3 Results and discussions

This chapter will present and discuss all the results proposed in the methodology. Firstly, the temperature obtained by the thermographic camera data will be presented, followed by the temperatures of the chip-tool interface obtained by the tool-workpiece thermocouple method.

Fig. 7 Schematical draw of the calibration of the tool-work-piece thermocouple in an oven

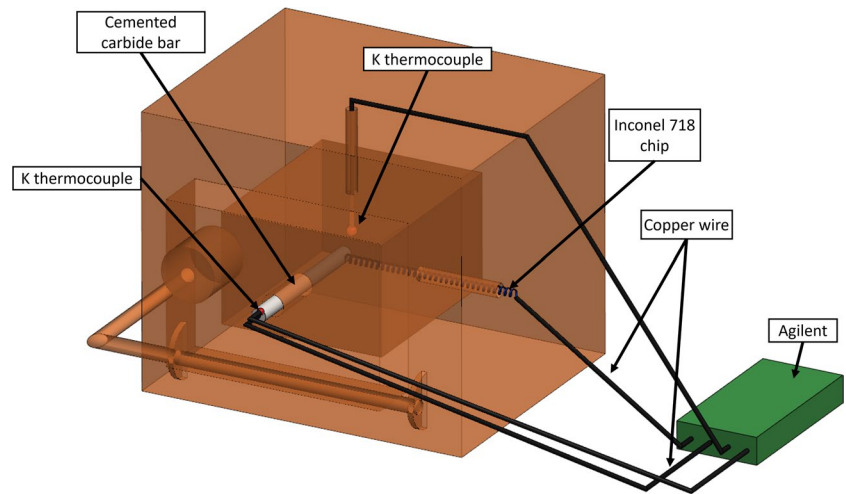


Table 6 Thermal camera temperature results

	Atmosphere	Coating	Depth of cut [mm]	Feed [mm/rev]	Cutting speed [m/min]	Temperature (T1) [°C]	Temperature (replica) [°C]	Average (T1 and T2) [°C]	Std. dev. [°C]
1	DM	TINAL	0.25	0.103	47	609	632	621	16
2	ICT	TINAL	0.25	0.103	94	612	617	615	4
3	ICT	TINAL	0.50	0.103	47	673	656	665	12
4	DM	TINAL	0.50	0.103	94	673	692	683	13
5	ICT	TINAL	0.25	0.297	47	613	634	624	15
6	DM	TINAL	0.25	0.297	94	697	663	680	24
7	DM	TINAL	0.50	0.297	47	674	682	678	6
8	ICT	TINAL	0.50	0.297	94	673	654	664	13
9	ICT	ALCRN+	0.25	0.103	47	636	647	642	8
10	DM	ALCRN+	0.25	0.103	94	652	669	661	12
11	DM	ALCRN+	0.50	0.103	47	653	664	659	8
12	ICT	ALCRN+	0.50	0.103	94	652	648	650	3
13	DM	ALCRN+	0.25	0.297	47	692	704	698	8
14	ICT	ALCRN+	0.25	0.297	94	611	650	631	28
15	ICT	ALCRN+	0.50	0.297	47	696	669	683	19
16	DM	ALCRN+	0.50	0.297	94	748	743	746	4

3.1 Temperature measured by the thermal camera

Table 6 and Fig. 8 display the average maximum temperatures obtained from thermal camera measurements for different cutting conditions, including initial tests and replicas. The thermal camera was positioned above the cutting zone, capturing the temperature of the upper chip-free surface.

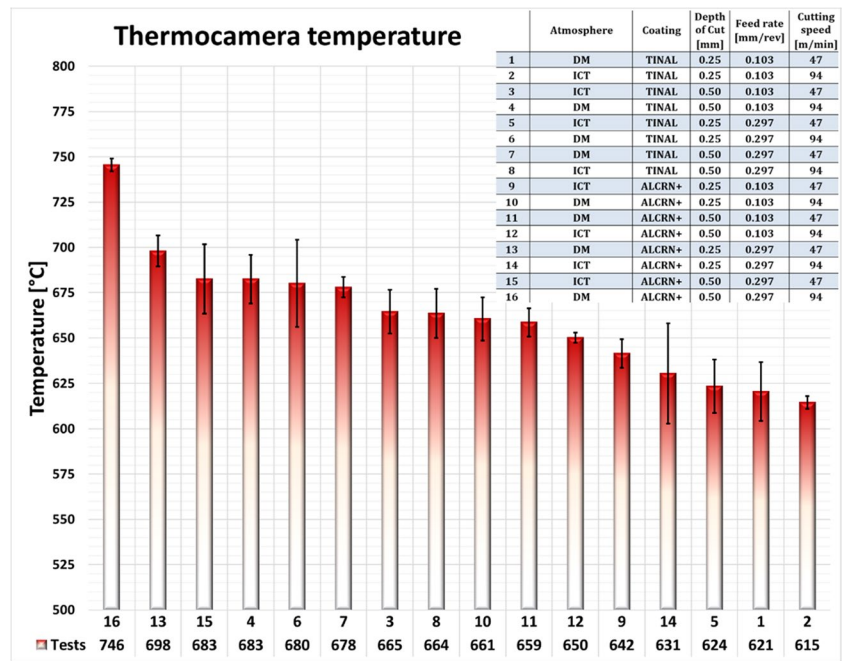
Figure 9 presents the Pareto chart showing the significant variables for a 95% reliability.

It was observed that by increasing the cutting parameters, there was also an increase in the machining temperature. A higher value of mechanical energy inevitably increases

the heat and, finally, the temperature. These results agree with several other works [57, 58]. Also, the coating of AlCrN+ and DM contributed to increasing it.

Figure 8 and Table 6 show that TiNAl and ICT had the lowest temperatures, averaging 615 ± 4 °C. In contrast, dry machining with the AlCrN+ coating resulted in the highest temperature of 746 ± 4 °C. TiNAl with ICT showed the lowest temperatures at 615 ± 4 °C, while dry machining with AlCrN+ resulted in the highest temperature at 746 ± 4 °C. These temperature values align with the findings of Zhao et al. [51] in a study on turning Inconel 718, where they observed a temperature around 750 °C during dry machining

Fig. 8 Thermal camera temperature results



using whisker-reinforced ceramic tools, although different from the cemented carbide tools used in this study.

Most input variables significantly influenced the machining temperature, except for cutting speed, an unexpected result that will be discussed further. Significant interactions were observed between cutting speed × cutting atmosphere and feed × cutting atmosphere. The depth of cut had the most pronounced effect on temperature, as shown in the Pareto chart in Fig. 9. Increasing the cut depth from 0.25 to 0.50 mm led to a significant temperature increase. This is attributed to higher cutting forces and increased power and energy conversion into heat. Although the heat dissipation area increased with a higher depth of cut, heat generation outweighed the dissipation area increase. Similar observations were made for the feed (*f*) and the interactions between cutting speed × atmosphere and feed × atmosphere. While cutting speed did not significantly affect temperature, increasing it from 47 to 94 m/min tended to raise the temperature.

Generally, higher cutting speeds lead to higher temperatures and lower cutting forces [59]. Nevertheless, Peixoto [43] used the ICT system when turning gray cast iron with uncoated cemented carbide tools and found that increasing the cutting speed reduced the cutting forces. França [42], using the same system and material, found that ICT could significantly (~22%) reduce the temperature in the tool-piece interface when turning cast-gray iron. So, a plausible hypothesis is that the ICT cooling capacity is high enough to reduce the cutting temperature, which would dim the cutting speed influence. Another factor corroborating this theory is that the atmosphere variable strongly influenced

the chip temperature. In addition, dry machining contributed to increasing it enormously. Further investigations are necessary to have a conclusive finding.

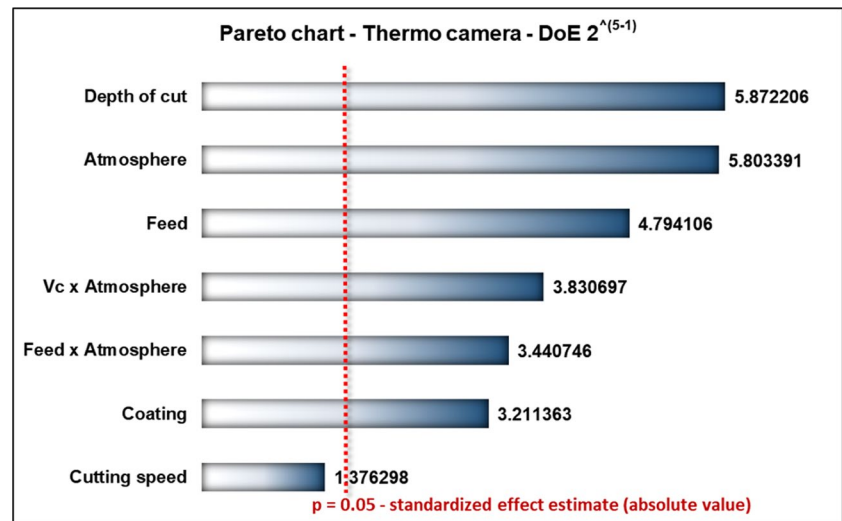
The influence of cutting parameters on machining temperature varies in the literature, indicating that temperature behavior depends on the specific machine-workpiece-tool setup. Korkut et al. [57] studied chip-back temperature while turning AISI 1117 steel using a thermal camera FLIR. They observed that increasing the depth of cut, feed, and cutting speed led to higher chip surface temperature, with cutting speed being the most influential parameter.

Kus et al. [60] obtained similar results in their study on hardened AISI 4140 alloy steel dry turning. They used thermocouples and an infrared sensor to measure temperature. Increasing cutting speed, feed, and depth of cut resulted in higher temperatures, with cutting speed having the most significant influence on temperature rise.

O’Sullivan and Cotterel [58] observed a decrease in machined surface temperature with higher feeds during the turning of aluminum alloy 6082-T6. Barbosa [38] used the same ICT system in turning hardened AISI D6 steel with PCBN tools and found that basic cutting parameters and cutting atmosphere did not significantly affect the machining temperature. However, cutting speed had the most significant influence, followed by cutting atmosphere and feed. Dry machining increased the temperature, while ICT reduced it, likely due to the system’s high heat removal capability.

Coating thickness significantly influenced its effect on temperature in machining processes but with more negligible effects than other variables. This study employed a

Fig. 9 Pareto chart results showing the influence of the input variables on the upper chip surface temperatures



simple TiNAl coating with a thickness of approximately 4 μm . The relatively thin nature of the TiNAl coating plays a significant role in its impact on temperature during machining. This distinction in thickness accounts for the observed differences in the results. While coatings with more substantial thickness can act as effective thermal insulators, the thinner TiNAl coating primarily serves other purposes in machining. It offers enhanced wear resistance and extended tool life, for instance. Thus, the smaller effect on temperature in this study can be attributed to the specific characteristics of the TiNAl coating, underlining the importance of coating thickness in its influence on temperature dynamics.

The temperature increased when using the double-coated AlCrN+ (level + 1) compared to the single-coated TiNAl (level – 1). Analytical studies by Kusiak et al. [61] comparing different coating types, including TiNAl, TiN, and Al_2O_3 , found that Al_2O_3 had the best thermal insulation properties. This supports the observation that TiNAl, a better thermal conductor than AlCrN+, effectively dissipates heat and reduces chip temperature. A study by Zhao et al. [62] supports these findings, highlighting the thermal barrier provided by AlCrN+ coating, which protects the substrate.

3.2 Temperature measured by the tool-workpiece thermocouple system

The chip-tool interface is the leading site of heat generation during machining, particularly in the secondary shear zone with high shear strains and deformation rates [5, 59, 63]. Friction and shearing in this zone cause rapid tool wear due to high temperatures. A tool-workpiece thermocouple system was calibrated following the procedures in Sect. 2.2 to measure the temperature accurately at the chip-tool

interface hot spot. The resulting calibration curve, Eq. 8, was obtained from three replication runs (Fig. 10), demonstrating a strong correlation (R^2 0.9868) between the measured temperatures and actual values.

$$\text{Temperature (T)} = 48.715x + 220 \text{ [}^\circ\text{C]} \quad (8)$$

where x is the $e.fs$ in [mV] generated by the chip-tool thermocouple system.

The results of the temperatures obtained during machining under several test conditions (test and replica) are presented in Table 7. The results are the average, measured with new tools. No test was performed with the tool presenting maximum flank wear higher than 0.1 mm ($V_B < 0.1\text{mm}$). Figure 11 presents these results graphically. With the results from the tool-workpiece thermocouple, the values for the average temperature of the chip-tool interface are determined [52].

ANOVA was performed for two cutting atmospheres: ICT \times DM and ICT \times CFA. Figure 12 presents a Pareto chart for ICT and DM, while Fig. 13 presents it for ICT and CFA. Both Pareto charts highlighted the variables significantly affecting the temperature with a 95% reliability index.

The study demonstrated a clear relationship between cutting parameters and the temperature at the tool-chip interface, indicating that increasing the cutting parameters resulted in higher temperatures. Temperature measurements obtained using the tool-workpiece thermocouple system, as shown in Fig. 11, compared different tool coatings and cutting atmospheres. The combination of TiNAl coating with CFA yielded the lowest temperature of 856 ± 17 $^\circ\text{C}$, while dry machining with AlCrN+ coating recorded the highest temperature of 1249 ± 8 $^\circ\text{C}$.

These temperature values' magnitude follows the results found by Marques [9]. The author machined Inconel 718 in turning operation using different atmospheres, such as

Fig. 10 Tool-workpiece thermo-couple calibration curves

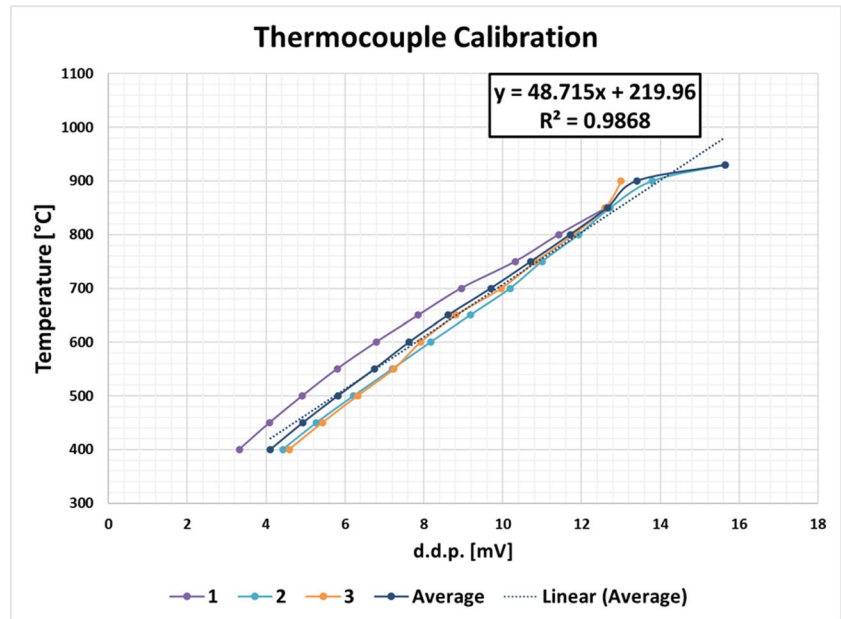
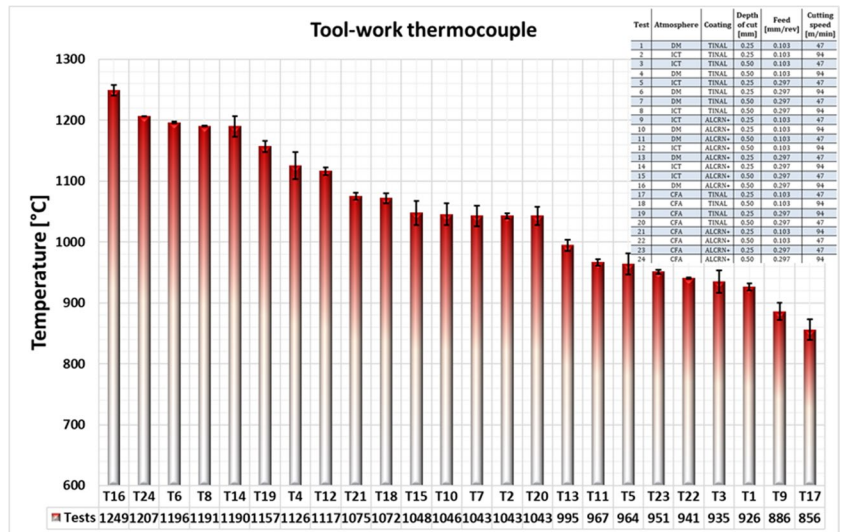


Table 7 Tool-work thermocouple temperature results

Test	Atmosphere	Coating	Depth of cut [mm]	Feed [mm/rev]	Cutting speed [m/min]	Temperature T1 [°C]	Temperature replica [°C]	Average (T1 and T2) [°C]	Standard dev. [°C]
1	DM	TINAL	0.25	0.103	47	922	930	926	6
2	ICT	TINAL	0.25	0.103	94	1046	1040	1043	4
3	ICT	TINAL	0.50	0.103	47	948	922	935	18
4	DM	TINAL	0.50	0.103	94	1110	1141	1126	22
5	ICT	TINAL	0.25	0.297	47	976	952	964	17
6	DM	TINAL	0.25	0.297	94	1197	1195	1196	1
7	DM	TINAL	0.50	0.297	47	1055	1031	1043	17
8	ICT	TINAL	0.50	0.297	94	1191	1190	1191	1
9	ICT	ALCRN+	0.25	0.103	47	876	896	886	14
10	DM	ALCRN+	0.25	0.103	94	1058	1033	1046	18
11	DM	ALCRN+	0.50	0.103	47	963	970	967	5
12	ICT	ALCRN+	0.50	0.103	94	1121	1112	1117	6
13	DM	ALCRN+	0.25	0.297	47	988	1001	995	9
14	ICT	ALCRN+	0.25	0.297	94	1178	1202	1190	17
15	ICT	ALCRN+	0.50	0.297	47	1034	1062	1048	20
16	DM	ALCRN+	0.50	0.297	94	1243	1255	1249	8
17	CFA	TINAL	0.25	0.103	47	844	868	856	17
18	CFA	TINAL	0.50	0.103	94	1077	1066	1072	8
19	CFA	TINAL	0.25	0.297	94	1150	1163	1157	9
20	CFA	TINAL	0.50	0.297	47	1032	1053	1043	15
21	CFA	ALCRN+	0.25	0.103	94	1070	1079	1075	6
22	CFA	ALCRN+	0.50	0.103	47	941	940	941	1
23	CFA	ALCRN+	0.25	0.297	47	953	949	951	3
24	CFA	ALCRN+	0.50	0.297	94	1207	1207	1207	0

Fig. 11 Tool-workpiece thermo-couple temperature results



MQL, CFA, and MQL + solid lubricants. The tools used were uncoated cemented carbides. The author found that by increasing the cutting speed from 20 to 70 m/min, the temperature was raised from 550 to 900 °C. Itakura et al. [64] used the same method for machining Inconel 718, turning operation, using multilayer coated carbide tools, P20 grade. They also found that with increasing cutting speed, the temperature increased proportionately. At 30 m/min, it was ~717 °C, and at 100 m/min 1, 046 °C.

As expected, dry machining exhibited the highest temperatures among all tested cutting conditions. However, CFA and ICT showed similar results, with a slight advantage of ICT over CFA at higher removal rates and larger machining parameters (doc, vc, and f). In contrast, CFA outperformed ICT at lower cutting conditions. This observation aligns with the theory that cutting fluid’s lubricating ability is more

effective at lower removal rates, while cooling becomes crucial at higher material removal rates [59, 63, 65]. This was surprising as the cutting fluids contain lubricating and cooling capacities acting together. Thus, CFA was expected to have a lower temperature as the ICT only has a cooling capacity.

Two hypotheses were proposed to explain the observed phenomenon. The first hypothesis suggests that at high cutting speeds, thin-film lubrication struggles to reach the tool-chip interface due to the absolute contact zone between the tool and chip, as well as the dynamic nature of the cutting process [66]. Cutting fluids serve two main purposes: lubrication and cooling. Lubrication is more effective at lower cutting conditions [67], while cooling becomes crucial at higher speeds [68].

Fig. 12 Pareto chart for temperature measured by the tool-workpiece thermocouple system (ICT×DM)

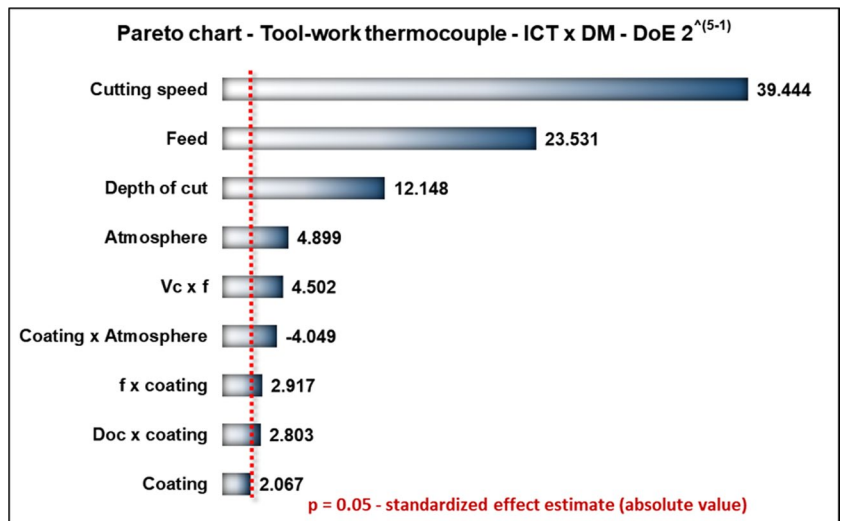
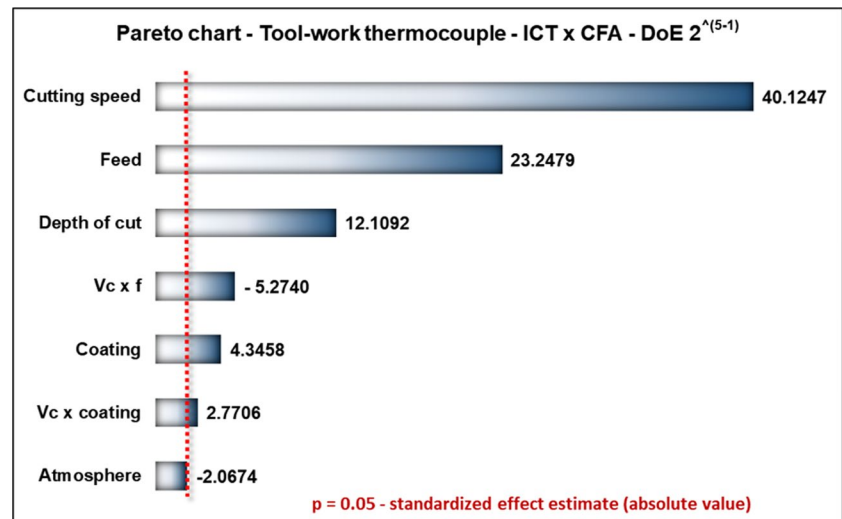


Fig. 13 Pareto's chart for temperature measured by the tool-workpiece thermocouple system (ICT×CFA)



The performance comparison between CFA and ICT supports the hypothesis that CFA exhibits better lubrication capacity at lower speeds but performs worse at higher speeds. This can be attributed to the increasing pressure between the tool and chip as machining parameters increase, forming a stronger adhesion zone characterized by absolute contact. Consequently, the cutting fluid faces challenges accessing the tool-chip interface, resulting in reduced performance [63].

ICT demonstrates its effectiveness as a highly efficient cooling method in such scenarios [59, 63, 65]. This finding aligns with the second hypothesis, which states that ICT compensates for the lack of lubrication by providing excellent heat removal capabilities, as discussed by Neto et al. [69]. Both hypotheses complement each other, suggesting that both phenomena likely coincide.

Generally, the AlCrN + coating exhibited higher temperatures compared to the TiNAl coating. The AlCrN + coating is known for its superior thermal insulation properties, contributing to its performance in high-temperature applications. These thermal insulation properties can be attributed to the unique microstructure and composition of the coating [70]. Compared to other coatings, such as TiNAl, AlCrN + exhibits enhanced resistance to heat flow. This characteristic enables the AlCrN + coating to act as a thermal barrier, reducing heat dissipation from the cutting zone and resulting in higher temperatures at the tool-chip interface. These results are consistent with the findings in the existing literature [14, 71–73].

In the statistical analysis comparing the cutting atmospheres of ICT and DM, Fig. 12, the most significant variables were cutting speed, feed, depth of cut, and atmosphere. Furthermore, significant interactions were observed between several variables that affected

the meaning of temperature increase (refer to Fig. 12). In summary, the use of DM contributed to an increase in the chip-tool interface temperature, particularly when combined with the AlCrN + coating and higher levels of basic cutting parameters such as cutting speed, feed, and depth of cut (v_c , f , and doc).

Considering ICT and DM, the results were under the literature [74], where generally, the v_c is the most influential parameter. Dry machining is critical when machining nickel-based superalloys because it has poor cooling and lubricating ability. It undoubtedly impacts the temperature by increasing it. Meanwhile, ICT has a high heat removal capacity, as proven by França [55]. The author found a temperature reduction at the tool-chip interface of almost 22% compared to dry cut when turning gray cast iron. He also found the atmosphere a significant influencing variable.

Considering ICT×CFA, in Fig. 13, similar findings were verified. The cutting speed, feed, and depth of cut were significant variables for the chip-tool interface temperatures, as were the interactions between cutting speed×feed and cutting speed×tool coating. The tool coating was a critical variable, with AlCrN + increasing the temperature. The cutting atmosphere had a marginal significance, i.e., almost was not significant. In this comparison, the ICT increased the chip-tool interface temperature as compared to CFA, however, only slightly. This is an exciting result, and the reasons were described previously.

To summarize, the higher the basic machining parameters (v_c , f , and doc), the higher the mechanical energy dispended, and the temperature will increase [63]. The results showed that the basic parameters were the most significant variables and had the higher parcel of contributions to increase the temperature at the tool-work interface. These are supported by Fernandes et al. [75] and Marques [9].

The coating was another significant factor influencing the temperature behavior. AlCrN is a natural thermal insulator, while TiAlN is an excellent conductor. Furthermore, a dual-layer coating was used in this study, with AlCrN deposited over TiAlN. The results concluded that this dual-layer coating effectively contributed to increased machining temperature.

Last but certainly not least, it has been demonstrated that internally cooled tools (ICT) have a superior ability to remove heat compared to dry machining and cryogenic applications. ICT maintain significantly lower temperatures than dry machining and are comparable to CFA. It is important to note that internally cooled tools are considered a form of dry machining, as highlighted by Neto et al. [69] and Fernandes et al. [39]. Consequently, ICT lacks the lubricating capacity of CFA. In cutting fluids, the oil acts as a lubricant on the rake face, facilitating sliding and reducing temperature. Therefore, it is reasonable to infer that ICT compensates for the lack of lubrication by having a much higher heat removal capacity, which ultimately results in comparable interface temperatures despite the absence of lubricating oil.

4 Conclusions

This study centered around the comparison of temperature within the proposed internally cooled tool (ICT) system with traditional cooling methods, namely dry machining (DM) and abundant coolant flood application (CFA). The main conclusions drawn from this investigation are as follows:

- Thermocamera tests revealed that the tool coating and the cutting atmosphere had the most significant impact, and TiAlN and ICT effectively lowered the chip temperature. Feed and cutting depth were also significant variables, while cutting speed surprisingly had no effect.
- In comparing ICT vs. CFA when using the tool-workpiece thermocouple system, the basic machining parameters (vc, f, and doc) were the most significant variables over the tool-workpiece interface temperatures. It can be concluded that ICT's cooling capacity corresponds to CFA's regarding chip temperature and tool interface despite the lack of lubrication.
- As for the tool-workpiece thermocouple for ICT vs. DM, ICT exhibited lower temperatures at the tool-workpiece interface due to higher heat removal in its internal channels, which exchange heat with the cooling fluid through convection.

Although further studies are required, the ICT system exhibited an excellent eco-friendly cooling technique for

machining. It demonstrates a noteworthy heat removal capability comparable to the industrial standard CFA method. The authors would greatly appreciate the emergence of fresh insights and the widespread adoption of the internally cooled tool (ICT) technology. This advancement holds the potential for substantial improvements in productivity and machining processes' sustainability. In pursuit of this goal, the authors encourage tool makers and scientists to embark on research endeavors to refine this innovative cooling method. This endeavor could lead to the creation of novel tool designs and the acquisition of valuable knowledge in the field.

Acknowledgements The authors would like to thank the following: The Grupo de Manufatura Sustentável (GMS) (Group of Manufatura Sustainable (GMS)) of the Laboratório de Ensino e Pesquisa em Usinagem (LEPU) at the Federal University of Uberlândia–Brazil; NipoTec–Special Tools; Walter Tools and Secco Tools; Villares Metals SA; Fiat Chrysler Automobiles (FCA). This work was supported by the Brazilian research agencies: Coordenação de Aperfeiçoamento de Pessoal de Nível Superior–Brasil (CAPES) (grant number 001, 2019), the Conselho Nacional de Desenvolvimento Científico e Tecnológico (CNPq) (grant number 001,2019), and Fundação de Amparo à Pesquisa do Estado de Minas Gerais (FAPEMIG) (grant number 001,2019).

Author contribution Gustavo Henrique Nazareno Fernandes: conceptualization, methodology, validation, formal analysis, investigation, writing—original draft, visualization, project administration.

Lucas Melo Queiroz Barbosa: validation, investigation, data curation, writing—review and editing.

Pedro Henrique Pires França: validation, investigation, data curation.

Eduardo Ramos Ferreira: validation, investigation, data curation.

Paulo S. Martins: funding acquisition; supervision; writing—review and editing; project administration.

Álison R. Machado: writing—review and editing; supervision; project administration.

Notice: Some parts of this article were rewritten with the help of artificial intelligence to improve writing fluency.

Funding This study was funded by Tupy S.A. which provided the work material, Walter Tools donated the tools, Nipo-Tec Ferramentas Industriais designed and machined the channels of the ICT inserts by REDM, and Brazilian research agencies CNPq, FAPEMIG, and Coordenação de Aperfeiçoamento de Pessoal de Nível Superior—Brasil (CAPES)—Finance Code 001 financially supported.

Data availability The datasets obtained during the current work are available from the corresponding author upon request.

Code availability Not applicable.

Declarations

Competing interests The authors declare no competing interests.

Ethics approval This article requires informed consent of the authors; it does not have any disclosure of potential conflicts of interest and does not involve human and/or animal participants.

Consent to participate The authors declare they consent to participate in this paper.

Consent to publish The authors declare they consent to publish this paper.

References

- Mahesh K, Philip JT, Joshi SN, Kuriachen B (2021) Machinability of Inconel 718: A critical review on the impact of cutting temperatures. *Mater Manuf Process* 36:753–791. <https://doi.org/10.1080/10426914.2020.1843671>
- Schmidt AO, Roubik JR (1949) Distribution of heat generated in drilling. *Trans Am Soc Mech Eng* 71:245–248
- Shaw MC (1984) *Metal cutting principles*. Clarendon
- Kronenberg M (1966) *Theory and practice for operation and development of machining processes*. Machining Science and Application
- Klocke F, Kuchle A (2009) *Manufacturing processes*. Springer, Berlin. <https://link.springer.com/content/pdf/10.1007/978-3-642-36772-4.pdf>
- Grzesik W (2008) *Advanced machining processes of metallic materials: theory, modelling and applications*. Elsevier
- Jamil M, Zhao W, He N et al (2021) Sustainable milling of Ti–6Al–4V: A trade-off between energy efficiency, carbon emissions and machining characteristics under MQL and cryogenic environment. *J Clean Prod* 281:125374. <https://doi.org/10.1016/j.jclepro.2020.125374>
- da Veiga FL, Faria MIST, Coelho GC (2017) Superliga Inconel-718: Caracterização microestrutural e validação da base de dados termodinâmicos. *Cad UniFOA* 7:77–85. <https://doi.org/10.47385/cadunifoa.v7.n1%20Esp.2185>
- Marques A (2015) Torneamento de inconel 718 com aplicação de lubrificantes sólidos. Universidade Federal de Uberlândia. <https://doi.org/10.14393/ufu.te.2015.151>
- Roy S, Kumar R, Panda A, Das RK (2018) A brief review on machining of Inconel 718. *Mater Today Proc* 5:18664–18673. <https://doi.org/10.1016/j.matpr.2018.06.212>
- Yin Q, Liu Z, Wang B et al (2020) Recent progress of machinability and surface integrity for mechanical machining Inconel 718: a review. *Int J Adv Manuf Technol* 109:215–245. <https://doi.org/10.1007/s00170-020-05665-4>
- Mustafa G, Anwar MT, Ahmed A, et al (2022) Influence of machining parameters on machinability of Inconel 718—a review. *Adv Eng Mater* 24:. <https://doi.org/10.1002/adem.202200202>
- Rubaiee S, Danish M, Gupta MK et al (2022) Key initiatives to improve the machining characteristics of Inconel-718 alloy: experimental analysis and optimization. *J Mater Res Technol* 21:2704–2720. <https://doi.org/10.1016/j.jmrt.2022.10.060>
- Byers JP (ed) (2006) *Metalworking fluids*, 2nd edn. CRC Press. <https://doi.org/10.1201/9781420017731>
- Almeida Carvalho DO, da Silva LRR, de Souza FCR, França PHP, Machado AD, Costa ES, Fernandes GHN, da Silva RB (2022) Flooding application of vegetable-and mineral-based cutting fluids in turning of AISI 1050 steel. *Lubricants* 10:309. <https://doi.org/10.3390/lubricants10110309>
- Fernandes GHN, Barbosa LMQ (2022) Machining cooling techniques. Recife: Even3 Publicações. <https://doi.org/10.29327/559427>. <https://publicacoes.even3.com.br/book/machining-cooling-techniques-594275>
- Iturbe A, Hormaetxe E, Garay A, Arrazola PJ (2016) Surface integrity analysis when machining inconel 718 with conventional and cryogenic cooling. *Procedia Cirp* 45:67–70. <https://doi.org/10.1016/j.procir.2016.02.095>
- Salem A, Hopkins C, Imad M et al (2020) Environmental analysis of sustainable and traditional cooling and lubrication strategies during machining processes. *Sustainability* 12:8462. <https://doi.org/10.3390/su12208462>
- Ozcelik B, Kuram E, Cetin MH, Demirbas E (2011) Experimental investigations of vegetable based cutting fluids with extreme pressure during turning of AISI 304L. *Tribol Int* 44:1864–1871. <https://doi.org/10.1016/j.triboint.2011.07.012>
- Ishfaq K, Anjum I, Pruncu CI et al (2021) Progressing towards sustainable machining of steels: a detailed review. *Mater.* 14:18–5162. <https://doi.org/10.3390/ma14185162>
- Wu X, Li C, Zhou Z et al (2021) Circulating purification of cutting fluid: an overview. *Int J Adv Manuf Technol* 117:2565–2600. <https://doi.org/10.1007/s00170-021-07854-1>
- Benedicto E, Carou D, Rubio EM (2017) Technical, economic and environmental review of the lubrication/cooling systems used in machining processes. *Procedia Eng* 184:99–116. <https://doi.org/10.1016/j.proeng.2017.04.075>
- Sankaranarayanan R, Krolczyk GM (2021) A comprehensive review on research developments of vegetable-oil based cutting fluids for sustainable machining challenges. *J Manuf Process* 67:286–313. <https://doi.org/10.1016/j.jmapro.2021.05.002>
- Demirbas E, Kobya M (2017) Operating cost and treatment of metalworking fluid wastewater by chemical coagulation and electrocoagulation processes. *Process Saf Environ Prot* 105:79–90. <https://doi.org/10.1016/j.psep.2016.10.013>
- Wang X, Li C, Zhang Y et al (2022) Tribology of enhanced turning using biolubricants: A comparative assessment. *Tribol Int* 174:107766. <https://doi.org/10.1016/j.triboint.2022.107766>
- Wang X, Li C, Zhang Y et al (2020) Vegetable oil-based nanofluid minimum quantity lubrication turning: Academic review and perspectives. *J Manuf Process* 59:76–97. <https://doi.org/10.1016/j.jmapro.2020.09.044>
- Şirin E (2023) Evaluation of tribological performance of MQL technique combined with LN₂, CO₂, N₂ ecological cooling/lubrication techniques when turning of Hastelloy C22 superalloy. *Tribol Int* 188:108786. <https://doi.org/10.1016/j.triboint.2023.108786>
- de Carvalho PP, Fernandes GHN, Barbosa LMQ et al (2023) Different cooling strategies applied during the process of aluminum alloy boring. *Int J Adv Manuf Technol*. <https://doi.org/10.1007/s00170-023-11840-0>
- Guo S, Li C, Zhang Y et al (2017) Experimental evaluation of the lubrication performance of mixtures of castor oil with other vegetable oils in MQL grinding of nickel-based alloy. *J Clean Prod* 140:1060–1076. <https://doi.org/10.1016/j.jclepro.2016.10.073>
- Fernandes Gustavo et al (2021) Wear mechanisms of diamond-like carbon coated tools in tapping of AA6351 T6 aluminium alloy. *Procedia Manufacturing* 53:293–298
- Zhang J, Li C, Zhang Y et al (2018) Experimental assessment of an environmentally friendly grinding process using nanofluid minimum quantity lubrication with cryogenic air. *J Clean Prod* 193:236–248. <https://doi.org/10.1016/j.jclepro.2018.05.009>
- Swain S, Patra SK, Roul MK, Sahoo LK (2022) A short review on cooling process using compressed cold air by vortex tube in machining. *Mater Today Proc* 64:382–389. <https://doi.org/10.1016/j.matpr.2022.04.722>
- Chiou RY, Lu L, Chen JSJ, North MT (2007) Investigation of dry machining with embedded heat pipe cooling by finite element analysis and experiments. *Int J Adv Manuf Technol* 31:905–914. <https://doi.org/10.1007/s00170-005-0266-8>
- Kantharaj I, Hiran Gabriel DJ, Prakash JB, Mohanasundaram S (2021) Experimental investigation on heat pipe-assisted cooling during milling process of AISI 1040. *Lect Notes Mech Eng* 601–609. https://doi.org/10.1007/978-981-15-4745-4_53
- Meyers PG (1961) Tool cooling apparatus. Attorney: Vernon F. Hauschill. USA n. US3137184. Deposit: 05 Jul 1961,

- Concession: 16 June 1964, United States Patent Office, 1964. <https://patents.google.com/patent/US3137184A/en>
36. Jeffries NP, Zerkle RD (1970) Thermal analysis of an internally-cooled metal-cutting tool. *Int J Mach Tool Des Res* 10:381–399. [https://doi.org/10.1016/0020-7357\(70\)90019-3](https://doi.org/10.1016/0020-7357(70)90019-3)
 37. Zerkle RD (1971) Cooling system for cutting tools and the like. US3571877A. <https://patents.google.com/patent/US3571877>
 38. Barbosa LMQ, França PHP, Fernandes GHN et al (2023) Comparison of the performance of the internally cooled tool in closed circuit against standard PCBN tools in turning AISI D6 hardened. *Journal of Manufacturing Process*
 39. Nazareno Fernandes GH, Bazon VT, Queiroz Barbosa LM et al (2023) Performance comparison between internally cooled tools and flood cooling during grey cast iron turning. *J Manuf Process* 85:817–831. <https://doi.org/10.1016/j.jmapro.2022.11.040>
 40. Wei X (2019) Novel turning tool with an internal cooling system. The University of Manchester, United Kingdom. <https://www.proquest.com/openview/da3066549b8283bc5e064eff2df6e564/1?pq-origsite=gscholar&cbl=2026366&diss=y>
 41. Rozzi JC, Chen W, Chen EE (2011) U.S. Patent No. 8,061,241. U.S. Patent and Trademark Office, Washington, DC
 42. França PHP, Barbosa LMQ, Fernandes GHN et al (2022) Thermal analysis of a proposed internally cooled machining tool system. *Int J Adv Manuf Technol*. <https://doi.org/10.1007/s00170-022-10602-8>
 43. Peixoto A (2021) Análise da força de corte e rugosidade no torneamento de ferro fundido cinzento utilizando sistema de resfriamento interno da ferramenta (Analysis of cutting force and roughness in gray cast iron turning using internal tool cooling system). Universidade Federal de Uberlândia. <https://doi.org/10.14393/ufu.di.2021.5592>
 44. ASM International (1990) ASM Handbook, vol 2. Nonferrous Alloys and Special-Purpose Materials, Properties and Selection
 45. Ceratizit (2022) CNMG. In: webpage. <https://cuttingtools.ceratizit.com/ie/en/products/7500363000.html?referrer=https%3A%2F%2Fwww.google.com%2F>. Accessed 11 Apr 2022
 46. Meola, C., & Carlomagno, G. M. (2004). Recent advances in the use of infrared thermography. *Measurement science and technology*, 15(9), R27. <https://doi.org/10.1088/0957-0233/15/9/R01>
 47. Da Silva LRR, Filho AF, Costa ES et al (2018) Cutting temperatures in end milling of compacted graphite irons. *Procedia Manufacturing*. Elsevier B.V., pp 474–484. <https://doi.org/10.1016/j.promfg.2018.07.056>
 48. da Silva MB, Wallbank J (1999) Cutting temperature: prediction and measurement methods—a review. *J Mater Process Technol* 88:195–202. [https://doi.org/10.1016/S0924-0136\(98\)00395-1](https://doi.org/10.1016/S0924-0136(98)00395-1)
 49. Davoodi B, Hosseinzadeh H (2012) A new method for heat measurement during high speed machining. *Measurement* 45:2135–2140. <https://doi.org/10.1016/j.measurement.2012.05.020>
 50. Dubey V, Sharma AK, Singh RK (2021) A technological review on temperature measurement techniques in various machining processes. *Advances in Metrology and Measurement of Engineering Surfaces: Select Proceedings of ICFMMP 2019*. pp 55–67. https://doi.org/10.1007/978-981-15-5151-2_6
 51. Zhao J, Liu Z, Wang B et al (2018) Cutting temperature measurement using an improved two-color infrared thermometer in turning Inconel 718 with whisker-reinforced ceramic tools. *Ceram Int* 44:19002–19007. <https://doi.org/10.1016/j.ceramint.2018.07.142>
 52. Kaminise AK, Guimarães G, da Silva MB (2014) Development of a tool–work thermocouple calibration system with physical compensation to study the influence of tool-holder material on cutting temperature in machining. *Int J Adv Manuf Technol* 73:735–747. <https://doi.org/10.1007/s00170-014-5898-0>
 53. Agapiou JS, Stephenson DA (1994) Analytical and experimental studies of drill temperatures. *Anal Eng Indust* 116(1):54–60. <https://doi.org/10.1115/1.2901809>
 54. Astakhov VP, Outeiro J (2019) Importance of temperature in metal cutting and its proper measurement/modelin. *Measurement in Machining and Tribology* 1–47. https://doi.org/10.1007/978-3-030-03822-9_1
 55. França PHP (2021) Estudo da temperatura em ferramentas de usinagem com canais de refrigeração internos no torneamento do ferro fundido cinzento. Dissertação (Mestrado em Engenharia Mecânica). Universidade Federal de Uberlândia, Uberlândia. <https://doi.org/10.14393/ufu.di.2021.283>
 56. Lima Júnior EDE (2020) Medição da temperatura de corte no torneamento do aço-ferramenta AISI D6 temperado e revenido auxiliado por LN2. 2020. 135f. Dissertação (Mestrado em Engenharia Mecânica). Centro de Tecnologia, Universidade Federal do Rio Grande do Norte, Natal. <https://repositorio.ufrn.br/handle/123456789/28897>
 57. Korkut I, Boy M, Karacan I, Seker U (2007) Investigation of chip-back temperature during machining depending on cutting parameters. *Mater Des* 28:2329–2335. <https://doi.org/10.1016/j.matdes.2006.07.009>
 58. O’Sullivan D, Cotterell M (2002) Workpiece temperature measurement in machining. *Proc Inst Mech Eng Part B J Eng Manuf* 216:135–139. <https://doi.org/10.1243/0954405021519645>
 59. Trent EM, Wright PK (2000) *Metal cutting*, 4th edn. Butterworth-Heinemann
 60. Kus A, Isik Y, Cakir MC et al (2015) Thermocouple and infrared sensor-based measurement of temperature distribution in metal cutting. *Sensors* 15:1274–1291. <https://doi.org/10.3390/s150101274>
 61. Kusiak A, Battaglia J-L, Rech J (2005) Tool coatings influence on the heat transfer in the tool during machining. *Surf Coatings Technol* 195:29–40. <https://doi.org/10.1016/j.surfcoat.2005.01.007>
 62. Zhao J, Liu Z, Wang B et al (2021) Tool coating effects on cutting temperature during metal cutting processes: comprehensive review and future research directions. *Mech Syst Signal Process* 150:107302. <https://doi.org/10.1016/j.ymssp.2020.107302>
 63. Machado AR, Coelho RT, Abrão AM, da Silva MB (2015) Teoria da usinagem dos materiais. Editora Blucher
 64. Itakura, K., Kuroda, M., Omokawa, H., Itani, H., Yamamoto, K., & Ariura, Y. (1999). Wear mechanism of coated cemented carbide tool in cutting of Inconel 718 super-heat-resisting alloy. *International Journal of the Japan Society for Precision Engineering*, 33(4), 326–332.
 65. Klocke E (1997) Dry cutting. *Cirp Ann* 46:519–526. [https://doi.org/10.1016/S0007-8506\(07\)60877-4](https://doi.org/10.1016/S0007-8506(07)60877-4)
 66. Fernandes GHN, Barbosa LMQ (2022) Heat in machining. In: Fernandes GHN, Barbosa LMQ (eds) *Machining cooling techniques an introduction*, 1st edn. Even3, Recife, pp 10–24. <https://doi.org/10.29327/559427.1-1>
 67. Kelly JF, Cotterell MG (2002) Minimal lubrication machining of aluminium alloys. *J Mater Process Technol* 120:327–334. [https://doi.org/10.1016/S0924-0136\(01\)01126-8](https://doi.org/10.1016/S0924-0136(01)01126-8)
 68. Amigo FJ, Urbikain G, Pereira O et al (2020) Combination of high feed turning with cryogenic cooling on Haynes 263 and Inconel 718 superalloys. *J Manuf Process* 58:208–222. <https://doi.org/10.1016/j.jmapro.2020.08.029>
 69. Neto, R. R. I., Fragelli, R. L., Fiocchi, A. A., Scalon, V. L., & de Angelo Sanchez, L. E. (2015). Toolholder Internally Cooled by a Phase Change Fluid in Turning of SAE. *Applied Mechanics and Materials*, 798, 486–490.
 70. BALZERS, Oerlikon (org.) (2023) BALINIT ALNOVA: reliable milling of the most demanding materials. Reliable milling

- of the most demanding materials. Oerlikon Balzers. Available from: <https://www.oerlikon.com/balzers/sg/en/portfolio/balzers-surfce-solutions/pvd-and-pacvd-based-coating-solutions/balinit/alcrnbased/balinit-alnova/>. Accessed 30 Aug 2023
71. Haapala KR, Zhao F, Camelio J, Sutherland JW, Skerlos SJ, Dornfeld DA, Rickli JL (2013) A review of engineering research in sustainable manufacturing. *Journal of manufacturing science and engineering* 135(4):041013. <https://doi.org/10.1115/1.4024040>
 72. OECD, P. B. (2009) Sustainable manufacturing and eco-innovation: towards a green economy. Policy Brief-OECD Observer
 73. Hsien WLY (2015) Towards green lubrication in machining. Springer, Singapore, p 7
 74. Palanikumar K, Boppana SB, Natarajan E (2023) Analysis of chip formation and temperature measurement in machining of titanium alloy (Ti-6Al-4V). *Exp Tech* 47:517–529. <https://doi.org/10.1007/s40799-021-00537-2>
 75. Fernandes Gustavo et al (2023) Towards green machining: wear analysis of a novel eco-friendly cooling strategy for Inconel 718. *Int J Adv Manuf Technol*. <https://doi.org/10.1007/s00170-023-12207-1>

Publisher's Note Springer Nature remains neutral with regard to jurisdictional claims in published maps and institutional affiliations.

Springer Nature or its licensor (e.g. a society or other partner) holds exclusive rights to this article under a publishing agreement with the author(s) or other rightsholder(s); author self-archiving of the accepted manuscript version of this article is solely governed by the terms of such publishing agreement and applicable law.